4-6-2016

Parametric analysis of a solid oxide fuel cell auxiliary power unit operating on syngas produced by autothermal reforming of hydrocarbon fuels

Jun Dong
Harbin Institute of Technology

Xinhai Xu
Harbin Institute of Technology

Ben Xu
The University of Texas Rio Grande Valley, ben.xu@utrgv.edu

Shuyang Zhang
University of Arizona

Parametric analysis of a solid oxide fuel cell auxiliary power unit operating on syngas produced by autothermal reforming of hydrocarbon fuels

Jun Dong,[1] Xinhai Xu,[1,a)] Ben Xu,[2] and Shuyang Zhang[2]
[1]*School of Mechanical Engineering and Automation, Harbin Institute of Technology Shenzhen Graduate School, Shenzhen 518055, China*
[2]*Department of Aerospace and Mechanical Engineering, University of Arizona, Tucson, Arizona 85721, USA*

(Received 10 November 2015; accepted 23 March 2016; published online 4 April 2016)

A 1 kW_e integrated auxiliary power unit (APU) system consisting of an autothermal reformer and a solid oxide fuel cell (SOFC) unit, as well as balance-of-plant components, was designed and analyzed. A relatively easy-to-approach SOFC model was developed in order to conveniently calculate V-I and P-I curves and the system's net efficiency at different operating conditions. The effects of steam to carbon and oxygen to carbon ratios in the reactants, channel dimensions of the SOFC unit, and hydrocarbon fuel types on the integrated APU system's performance were discussed. Five hydrocarbon fuels including diesel, Jet-A, gasoline, ethanol, and methanol were studied as fuel sources for the APU system. The system's net efficiency around 35% is possible for all the tested fuels in the current density range of 100–400 mA/cm^2. The APU system was also verified to be thermally self-sustainable in the steady state operation by a thermal management analysis. © *2016 AIP Publishing LLC*.
[http://dx.doi.org/10.1063/1.4945572]

NOMENCLATURE

Roman letters

A	surface area, m^2
D	diffusivity, m^2/s
d_h	hydraulic diameter, m
$\dot{E}$	power, W
F	Faraday constant, C/mol
h	convection mass transfer coefficient, m/s
H	enthalpy, J/mol
I	current density, mA/cm^2
k_B	Boltzmann constant, eV/K
$\dot{m}$	mass flow rate, kg/s
M	molecular weight, g/mol
$\dot{n}$	mole flow rate, mol/s
P	pressure, Pa
r	resistivity, Ω m
R	gas constant, J/mol K
R_p	pore radius, m
Sh	Sherwood number
T	temperature, K

a)Author to whom correspondence should be addressed. Electronic mail: xuxinhai@hitsz.edu.cn

U overall mass transfer resistance, s/m
X mole fraction
ΔG Gibbs free energy change, kJ/mol

Greek letters

ε porosity
η activation polarization overpotential, V
v atomic diffusion volume
ρ mass concentration, kg/m^3
σ ionic conductivity, S/cm
τ tortuosity

Subscripts

a anode
b bulk flow
c cathode
eff effective
int interface
K Knudson
mt mass transfer

Superscripts

a anode
c cathode
i species i
0 standard condition at 1 atm

I. INTRODUCTION

Solid oxide fuel cell (SOFC) can produce clean electric power at a relatively high efficiency by using hydrogen or syngas as energy source. The characteristics of high operating temperature (650–1000 °C), sulfur tolerance, and ability to utilize CO make SOFCs promising for onboard auxiliary power unit (APU) applications in vehicles, aircraft, and ships.[1–4] Hydrogen or syngas can be obtained by reforming of liquid hydrocarbon fuels. Recently, an onboard fuel reforming system has been proposed to convert various types of fuels into hydrogen or syngas.[5] By introducing the onboard fuel reforming system to fuel cell APUs, problems such as lack of hydrogen production and storage infrastructures are resolved.[6,7]

Three commonly used reforming approaches are steam reforming (SR), partial oxidation (POX), and autothermal reforming (ATR). ATR is preferred for onboard fuel reforming systems due to its advantages of thermally neutral reactions, compact size, and favorable H_2/CO ratio in the reformate.[8,9] ATR of traditional logistic fuels (gasoline, diesel, and jet fuels) and alternative fuel candidates (ethanol and methanol) has been studied.[10–18] In the dry reformates, H_2 concentration is generally in the range of 30%–40%, and CO content is usually within 10%–15%. However, in practical operation of a SOFC APU, wet reformate containing high temperature steam instead of dry reformate is fed into the FC unit to avoid energy loss during cooling. Therefore, H_2 and CO concentrations in the wet reformate are lower than those in the dry reformate because of the presence of large quantity steam.[19] SOFC's performance with the wet reformate fed into the anode side as the energy source needs to be studied. The parameters which could affect the SOFC and APU system's performance need to be investigated. Fuel adaptability of the integrated APU system is also important for commercialization.[16,20]

In the present study, a 1D SOFC model was developed to analyze the performance of a 1 kW$_e$ integrated APU system consisting of SOFC units and an ATR reformer. The SOFC units

were operated on the syngas produced from the ATR reformer. The effects of the steam to carbon (S/C) and the oxygen to carbon (O_2/C) ratios in the reactants and channel dimensions of the SOFC unit on the system's performance with regard to V-I and P-I curves and efficiencies were studied based on the model. Fuel adaptability of this APU system for several fuels, including gasoline, diesel, Jet-A fuel, ethanol, and methanol, were also investigated with respect to V-I and P-I curves and efficiencies. In the last system, thermal management analysis considering all the balance-of-plant (BoP) components was conducted to verify the self-sustainability of the integrated APU system.

II. INTEGRATED APU SYSTEM AND SOFC MODELING

A. APU system

Figure 1 shows the process flow diagram of the SOFC APU system combined with an ATR reformer. Besides the SOFC units and the reformer, the complete system also has BoP components, including pumps, air blower, heat exchangers (HE), and an after burner for burning anode off-gas. In the steady state operation of the integrated APU system, fuel, water, and air at room temperature are supplied at constant flow rates by pumps and air blower. Before injecting into the reformer, the reactants are pre-heated to the required temperatures. Detailed reformer design and picture of the lab-scale ATR reformer are shown in our previous paper.[13] Dry reformate compositions are analyzed by a Gas Chromatography (GC) system equipped with a thermal conductivity detector (TCD). After the reformer, high temperature ($\sim$700 °C) wet reformate is fed into the SOFCs to produce electric power. The SOFC's performance, including output voltage and power density, are calculated based on the modeling analysis discussed in Section II B. As SOFCs are used in the integrated system, CO clean-up components such as high and low temperature water-gas-shift (WGS) reactors and preferential oxidation (Prox) reactor are unnecessary, which largely reduces the complexity of the system and increases the system's net efficiency. A portion of the electric power produced by the SOFC units is consumed by the pumps and air blower. Exhaust heat in the FC off-gas and heat produced by combustion of the unreacted H_2 in the after burner are used for pre-heating of fuel, water, and air. An effective thermal management is important in the combined system regarding its self-sustainability.

Three different efficiencies—energy conversion efficiency for the reformer, electric power output efficiency for the SOFCs, and the system's net efficiency—are discussed for the APU system. Their definitions are shown as follows:

$$\text{Energy conversion efficiency}\,(\%) = \frac{\dot{n}_{H_2}\text{LHV}_{H_2} + \dot{n}_{CO}\text{LHV}_{CO}}{\dot{n}_{C_mH_nO_z}\text{LHV}_{C_mH_nO_z}} \times 100, \tag{1}$$

$$\text{SOFC efficiency}\,(\%) = \frac{W_{elec}}{\dot{n}_{H_2}\text{LHV}_{H_2} + \dot{n}_{CO}\text{LHV}_{CO}} \times 100, \tag{2}$$

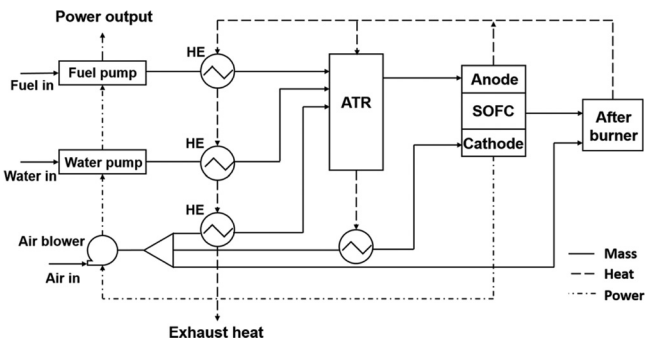

FIG. 1. Process flow diagram of the integrated system.

TABLE I. Chemical formula and LHVs of the tested fuels.

	Gasoline	Diesel	Jet-A	Methanol	Ethanol
Average chemical formula	C_8H_{18}	$C_{14}H_{26}$	$C_{11.6}H_{22.3}$	CH_3OH	C_2H_5OH
Lower heating value (MJ/kg)	44.4	43.4	43.26	19.93	28.86

$$\text{Net system efficiency}\,(\%) = \frac{W_{elec} - W_{BoP}}{\dot{n}_{C_mH_nO_z}\text{LHV}_{C_mH_nO_z}} \times 100, \tag{3}$$

where $C_mH_nO_z$ represents the fuel, and the average chemical formula used for gasoline, diesel, and Jet-A fuel is shown in Table I. $\dot{n}$ is molar flow rate (mol/s), and LHV is lower heating value (kJ/mol). W_{elec} (kW) is the electric power produced by SOFC, and W_{BoP} (kW) is the power consumed by BoP components.

B. SOFC modeling

A 1D model of an anode-supported SOFC was developed by taking into account of concentration polarization, activation polarization, and ohmic loss. Theoretically, the output voltage of the SOFC equals to the equilibrium electromotive force deducted by activation polarization overpotentials and ohmic loss.[21,22] In the anode side, H_2 and CO transport from the bulk flow to the anode and electrolyte interface through mass convection and diffusion. At the anode catalyst, CO is converted to H_2 by WGS reaction due to the fact that WGS reaction is more favorable than the direct oxidation of CO. H_2 reacts with oxide ions, which are formed by cathode reaction and transport through the electrolyte, to form water. Electrons are released, and they migrate to the cathode side through the external circuit. The parameters used for the SOFC modeling are selected from the literature and listed in Table II.

TABLE II. Operating conditions for modeling of the SOFC.[23–27]

Operating temperature (°C)	700
Operating pressure (kPa)	220
Fuel utilization factor	0.85
Oxygen utilization factor	0.2
Oxygen fraction in air (%)	20.5
Nitrogen fraction in air (%)	79.4
Water vapor fraction in air (%)	0.1
Half channel width L_0 (mm)	4
Channel length (m)	0.1
Channel height (mm)	3
Pore radius of GDL (m)	2×10^{-5}
Pore radius of electrodes (m)	5×10^{-5}
Tortuosity of GDL and electrodes	5.9
Porosity of GDL and electrodes	0.5
Thickness of GDL (mm)	1
Thickness of anode (mm)	0.25
Thickness of cathode (mm)	0.05
Thickness of electrolyte (mm)	0.02
Contact resistivity ($\Omega\,m^2$)	1.7×10^{-6}
Resistivity of GDL ($\Omega\,m$)	7.837×10^{-6}
Transfer coefficient α	0.5

1. Concentration polarization

Electromotive force considering concentration polarization can be calculated by Nernst equation with concentration of each species in the electrode and electrolyte interface. In the model, the concentration of each species i is calculated separately following Eq. (4) in Table III. The overall mass transfer resistance U consists of three parts, which is calculated by Eq. (5). The convection mass transfer coefficient h and effective diffusivity D_{eff} are calculated by Eqs. (6) to (10), as shown in Table III.

In the anode side, WGS reaction also occurs besides the H_2 oxidation reaction due to the fact that a large amount of CO (∼10%) exists in the wet reformate. In the steady state operation, the amount of consumed CO can be obtained by calculating the equilibrium constant of the WGS reaction as shown in Eq. (11) in Table III.

2. Activation polarization

The activation polarization is estimated based on the Butler-Volmer equations[28] as shown in Eqs. (12) and (13) in Table III. The exchange current density I_0 is dependent on many factors, including material properties such as porosity and pore size, as well as operating conditions of temperature and pressure. z is the number of electrons transported through the external circuit with consumption of one mole hydrogen in the SOFC.[29] As identical transfer coefficient α is selected for anode and cathode, the Butler-Volmer equations become parabolic equations. Therefore, the activation polarization overpotential can be obtained by solving the parabolic Butler-Volmer equations.[30]

3. Ohmic loss

Figure 2 shows an equivalent electrical circuit, which is used to calculate the ohmic loss due to internal electricity conduction resistance. The contact resistance between the electrodes and the electrolyte is ignored. Therefore, the total resistance from the anode to the cathode includes contact resistance of the gas diffusion layers (GDLs) to the current collectors and the GDLs to the electrodes, conduction resistance in the in-plane and through-plane directions of the GDLs and the electrodes, as well as resistance in the YSZ electrolyte. Totally, fourteen nodes are used in the equivalent electrical circuit, and the electrical potential at each node is calculated based on the Kirchhoff's current law, which states that the total current flow at each node is zero. Using a similar method to calculate ohmic loss in SOFC has been reported in the literature.[30,31]

Contact resistivity is related to the topography of the contacting layers and channel geometry,[32] and its magnitude is usually in the order of $10^{-7}\,\Omega\,m^2$.[33] The anode resistivity and the cathode resistivity are calculated according to Eqs. (14) and (15) in Table III, respectively.[34,35] Ionic conductivity in the YSZ electrolyte is calculated by Eq. (16).[2]

4. Model validation

The SOFC model was validated by comparing calculated V-I and P-I curves with the experimental data reported by Lin *et al*. for an anode-supported SOFC.[36] Voltage output and power density of the SOFC were calculated at three different operating temperatures of 600, 650, and 700 °C, and they were compared with the measured values as shown in Figure 3. In the model validation calculation, the operating pressure was 1 atm, and pure hydrogen gas was supplied to anode. The anode thickness of 600 μm, electrolyte of 50 μm, and cathode of 20 μm were used as cell dimensions.[36] Figure 3 shows a good agreement between the calculated values and the experimental data, so that the developed model was validated.

III. RESULTS AND DISCUSSION

A. Effects of S/C and O_2/C ratios

The effects of S/C and O_2/C ratios in the reactants on the system's performance were studied using surrogate fuel *n*-dodecane as the energy source. The ATR reaction of *n*-dodecane is

TABLE III. Equations of the SOFC model.

$$\rho_b^i - \rho_{int}^i = \frac{\dot{m}_i U_i}{A_{mt}} \tag{4}$$

$$U_i = \frac{1}{h_i} + \frac{\delta_{GDL}}{D_{i,eff}^{GDL}} + \frac{\delta_{electrode}}{D_{i,eff}^{electrode}} \tag{5}$$

$$h_i = \frac{Sh \cdot D_i}{d_h} \tag{6}$$

$$D_i = \frac{1 - X_i}{\sum_{j \neq i} X_j / D_{ij}} \tag{7}$$

$$D_{ij} = \frac{0.0103 T^{1.75} \left(\frac{1}{M_i} + \frac{1}{M_j} \right)}{P \left[\nu_i^{1/3} + \nu_j^{1/3} \right]^2} \tag{8}$$

$$D_{i,eff} = \frac{\tau}{\varepsilon} \left(\frac{1}{D_{i,K}} + \frac{1}{D_{ij}} \right) \tag{9}$$

$$D_{i,K} = 97 R_p (T/M_i)^{1/2} \tag{10}$$

$$K_{WGS} = \exp\left(-\frac{\Delta G_{WGS}^0}{RT} \right) = \frac{\dot{n}_{CO_2}^{out} \dot{n}_{H_2}^{out}}{\dot{n}_{CO}^{out} \dot{n}_{H_2O}^{out}} \tag{11}$$

$$I = I_0^a \left[\exp\left(\frac{\alpha_a z F \eta_a}{RT} \right) - \exp\left(\frac{(1 - \alpha_a) z F \eta_a}{RT} \right) \right] \tag{12}$$

$$I = I_0^c \left[\exp\left(\frac{\alpha_c z F \eta_c}{RT} \right) - \exp\left(\frac{(1 - \alpha_c) z F \eta_c}{RT} \right) \right] \tag{13}$$

$$r_a = \left[95 \times 10^6 / T \exp\left(-1150/T \right) \right]^{-1} \tag{14}$$

$$r_c = \left[42 \times 10^6 / T \exp\left(-1200/T \right) \right]^{-1} \tag{15}$$

$$\sigma = 1.63 \times 10^2 \exp\left(\frac{-0.79\text{eV}}{k_B T} \right) \tag{16}$$

shown in Eq. (17). In the integrated APU system, S/C and O_2/C are two independent operating parameters which could influence the reformate compositions as well as the SOFC's performance. The effects of S/C in the range of 1.5–2.1 and O_2/C in the range of 0.42–0.48 were experimentally studied for ATR of *n*-dodecane in our previous paper.[13] Mole fractions of major species in the wet reformate and ATR energy conversion efficiency at different S/C and O_2/C

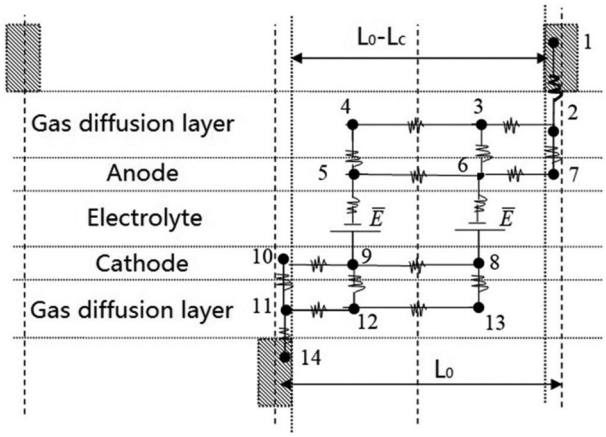

FIG. 2. Equivalent electrical circuit for ohmic loss analysis.

ratios are shown in Figure 4. O_2 and CH_4 are ignored because their mole fractions are both less than 0.1% in the wet reformate. In the tests with S/C = 1.8 and 2.1, the mole fraction of steam in the wet reformate is 5%–8% higher than that in the tests with S/C = 1.5, which suggests that excessive steam is fed into the reformer. The mole fractions of H_2 and CO are also lower in the cases with S/C = 1.8 and 2.1, which is caused by the dilution of the reformate with excessive steam. By varying O_2/C at a constant S/C of 1.5, mole fractions of H_2, CO, and CO_2 are relatively stable. The fraction of N_2 is high at O_2/C = 0.48 because excessive air is fed into the reformer. Figure 4(b) shows that the energy conversion efficiency is lower with excessive air or steam, but the efficiency only reduces less than 3%. Therefore, the reformer can run at a relatively wide operating ratios range as the energy conversion efficiency is insensitive to small change in the operating ratios.

$$C_{12}H_{26} + aO_2 + bH_2O \rightarrow (24 - 2a - b)CO + (2a + b - 12)CO_2 + (b + 13)H_2. \quad (17)$$

By using the wet reformate obtained at various S/C and O_2/C as the source gas, the performance of the SOFC unit was calculated based on the developed model. Figure 5(a) shows the calculated output voltage and power density at different current densities of the SOFC unit. S/C has more significant influence on output voltage and power density compared to O_2/C. The performance of the SOFC is almost the same at cases with an identical S/C = 1.5 and varying O_2/C, whereas output voltage and power density decrease slightly with increased S/C. The maximum power density is about 321 mW/cm^2 at 690 mA/cm^2, 315 mW/cm^2 at 680 mA/cm^2, and

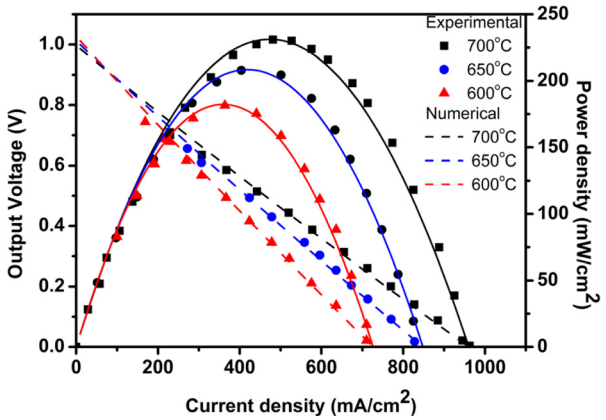

FIG. 3. Model validation (solid line: power density; dashed line: output voltage).

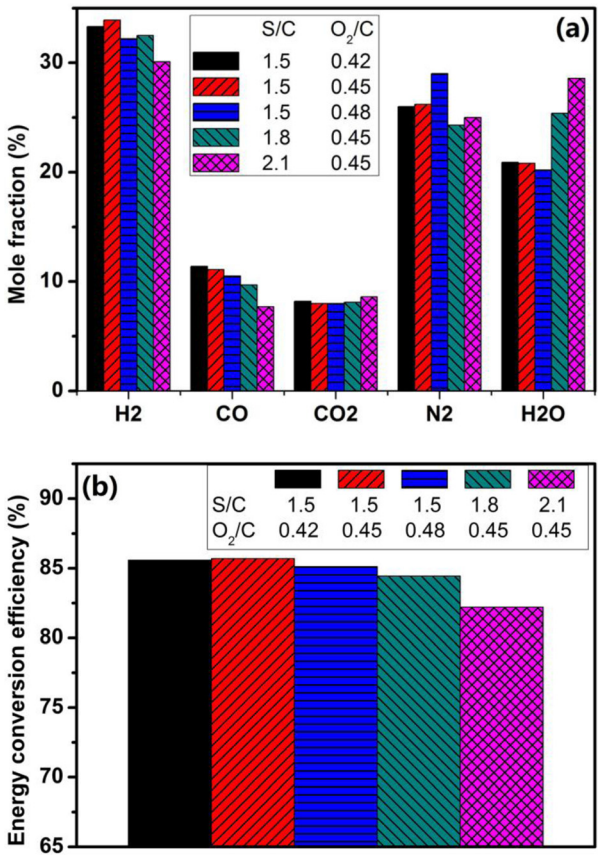

FIG. 4. (a) Wet reformate compositions and (b) reformer energy conversion efficiency at various ratios.

310 mW/cm^2 at 670 mA/cm^2 corresponding to S/C = 1.5, 1.8, and 2.1, respectively. This can be explained by the dilution of H_2 and CO concentrations caused by excess steam in the wet reformate, as shown in Figure 4(a). Figure 5(b) shows SOFC's efficiency and the system's net efficiency versus current density at various operating ratios. The difference of the SOFC's efficiency at different S/C and O_2/C is almost negligible, and the difference of the system's net efficiency at various ratios is within 4%, which is in agreement with the difference of the ATR energy conversion efficiency. The integrated APU system is also insensitive to a small change in S/C and O_2/C, so that it can operate in relatively wide operating ratios as well.

B. Effect of channel dimension

The effect of channel dimension of the SOFC unit on the APU system's performance was studied using desulfurized Jet-A fuel as the energy source. Hsieh and Chu[37] reported that the rib and channel geometric ratio has a significant influence on the performance of the fuel cell and an optimal rib-to-channel width ratio existed with respect to the fuel cell power density. In the present study, different values of R_{LC}, which is defined as the ratio of L_c and L_0 as shown in Figure 2, were selected for the SOFC's performance calculation. Six different R_{LC} from 0.20 to 0.45 were examined with fixed L_0 of 4 mm and H_c of 3 mm. Figure 6(a) shows the calculated V-I and P-I curves at different R_{LC}, and Figure 6(b) shows the SOFC's efficiency and the system's net efficiency at different R_{LC}. Figure 6(a) indicates that R_{LC} has a more significant impact on the SOFC's performance compared to the operating ratios of S/C and O_2/C. At a low current density region (<300 mA/cm^2), the difference of output voltage and power density at different R_{LC} is negligible, but the difference increases rapidly as the current density increases. The SOFC's performance at $R_{LC} = 0.40$ corresponds to the highest output voltage and power

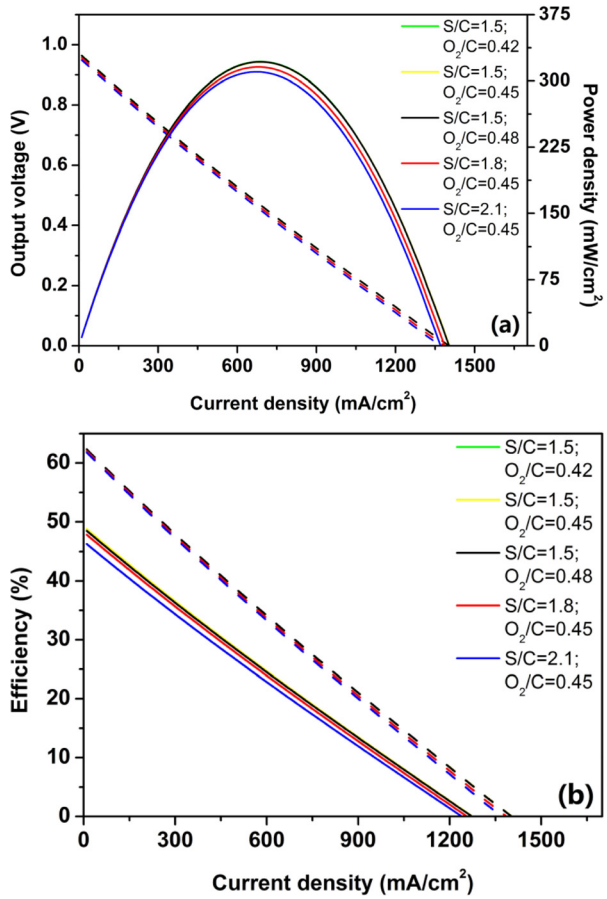

FIG. 5. (a) Calculated SOFC's performance, and (b) calculated efficiency of the SOFC and APU system (solid line: system's net efficiency; dashed line: SOFC's efficiency) at various ratios.

density among the tested conditions. At $R_{LC} = 0.20$, the maximum power density is only 297 mW/cm^2 at 630 mA/cm^2, but at $R_{LC} = 0.40$, the maximum power density increases to 346 mW/cm^2 at 740 mA/cm^2. The channel dimensions affect transportation of the reformate to the gas diffusion layer. A narrow channel rib width enhances the reformate transport because of the large surface area for mass transfer but also results in poor electron transfer. In contrast, a wide rib width is favorable for the electrical current conduction but limits reactants transportation.[37] Besides, too small rib width is difficult to fabricate by CNC machining. Consequently, an optimal R_{LC} was observed, as shown in Figure 6(a). The SOFC's highest efficiency and the system's net efficiency are also observed at the optimal R_{LC}, as shown in Figure 6(b). However, the difference of the system's net efficiency and the SOFC's efficiency at various R_{LC} is not huge. At the current density of 800 mA/cm^2, the difference of the system's net efficiency and the SOFC's efficiency at various R_{LC} are both within 5%.

C. Effect of fuel types

Fuel adaptability of the ATR reformer was already experimentally studied in our previous work, and the reformer was verified to be compatible with commonly used fuels, including diesel, Jet-A, gasoline, ethanol, and methanol.[16] Detailed ATR testing conditions for each fuel are listed in Table IV. For all the tested fuels, except Jet-A, the S/C and O_2/C ratios were not optimized for the reformer. Figure 7(a) shows the mole fraction of compositions in the wet reformate of each tested fuel. Figure 7(b) compares the energy conversion efficiency for ATR of different fuels. Figure 7(a) indicates that methanol has the highest mole fractions of H_2 and CO

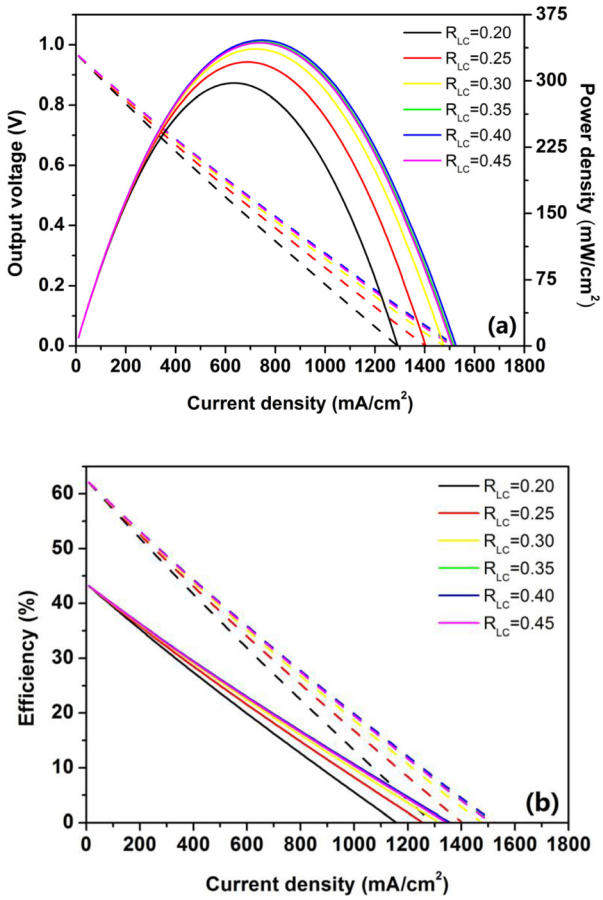

FIG. 6. (a) Calculated SOFC's performance, and (b) calculated efficiency of the SOFC and APU system (solid line: system's net efficiency; dashed line: SOFC's efficiency) at different R_{LC}.

compared to other fuels. A similar result for ATR of methanol was reported by Nilsson *et al.*[20] The mole fraction of N_2 is lower for ethanol and methanol because low O_2/C was used in ATR of these fuels as shown in Table IV. Mole fraction of H_2O for ethanol is the highest since the S/C ratio used was the highest for ATR of ethanol. Methanol also shows a high mole fraction of H_2O, although its S/C is lower than diesel and gasoline. Jet-A has the least mole fraction of H_2O in its wet reformate due to the lowest S/C used in ATR of Jet-A. Jet-A also shows relatively high mole fractions of H_2 and CO because its operating ratios were already optimized. Diesel and gasoline have similar mole fraction of each species in their wet reformate because they were tested at identical operating conditions. Figure 7(b) shows that the highest reformer energy conversion efficiency is obtained for methanol since its wet reformate has the highest

TABLE IV. ATR operating conditions for five hydrocarbon fuels.

		Pre-heating temperature (°C)					
Fuel	Fuel flow rate (ml/min)	Steam	Air	Fuel	S/C	O_2/C	GHSV
Diesel	5.4	250	175	140	2.0	0.40	42 850
Jet-A	6.0	250	175	140	1.5	0.45	35 980
Gasoline	6.1	250	175	120	2.0	0.40	41 370
Ethanol	8.6	250	175	25	3.0	0.35	62 630
Methanol	12.4	250	175	25	1.7	0.20	59 250

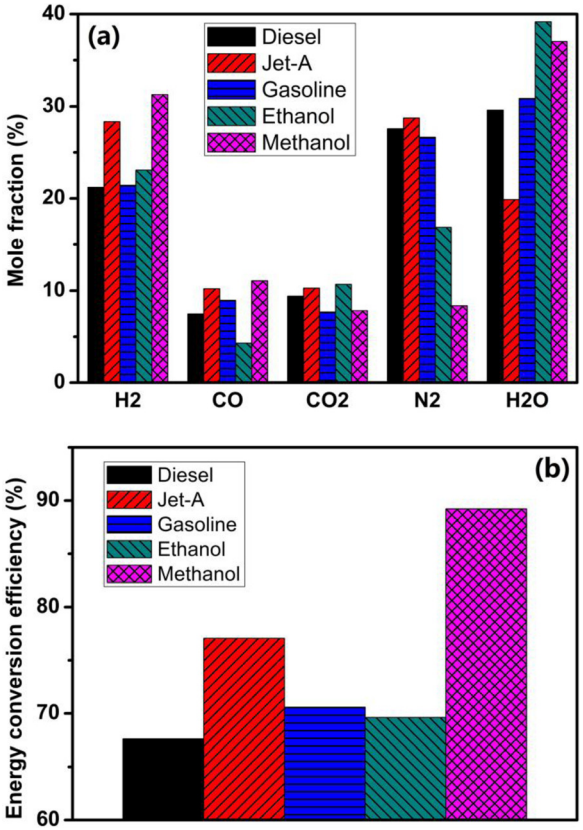

FIG. 7. (a) Mole fractions of compositions in the wet reformates and (b) reformer energy conversion efficiency for ATR of different fuels.

mole fractions of H_2 and CO. Jet-A has the second highest energy conversion efficiency because the ATR operating conditions were optimized as reported in our previous study.[13] The lowest energy conversion efficiency for diesel is 67%, and the highest energy conversion efficiency for methanol is 89%. The energy conversion efficiency is 77%, 70%, and 69% for Jet-A, gasoline, and ethanol, respectively.

Figure 8(a) shows the calculated V-I and P-I curves of the SOFC operating on the wet reformates of different fuels. Figure 8(b) shows the SOFC's efficiency and the system's net efficiency for different fuels. It can be seen from Figure 8(a) that SOFC's performance based on wet reformates of different fuels is similar, except that Jet-A has a slightly better performance than other fuels. The maximum power density for Jet-A is 346 mW/cm^2 at 740 mA/cm^2. Ethanol has the lowest maximum power density in the five tested fuels, which is 324 mW/cm^2 at 710 mA/cm^2. The difference is only 22 mW/cm^2. Figure 8(b) shows that the SOFC's efficiency is almost identical for all the tested fuels, so that the APU system's net efficiency is largely affected by the reformer energy conversion efficiency. In the current density range of 100–400 mA/cm^2, the system's net efficiency of 34%–45%, 30%–40%, 25%–35%, 25%–35%, and 24%–34% can be achieved for methanol, Jet-A, ethanol, gasoline, and diesel, respectively. In the same current density range, the output voltage is about 0.7–0.9 V, and the power density is about 90–270 mW/cm^2 for all the tested fuels. As the LHV of each fuel supplied to the APU system is about 3.25 kW_t, the output electrical power is higher than 1 kW_e if the system's net efficiency is larger than 30%.

D. System thermal management

Thermal management of the integrated APU system was studied by calculating the heat consumed and heat produced in each component. The SOFC unit is assumed to be adiabatic

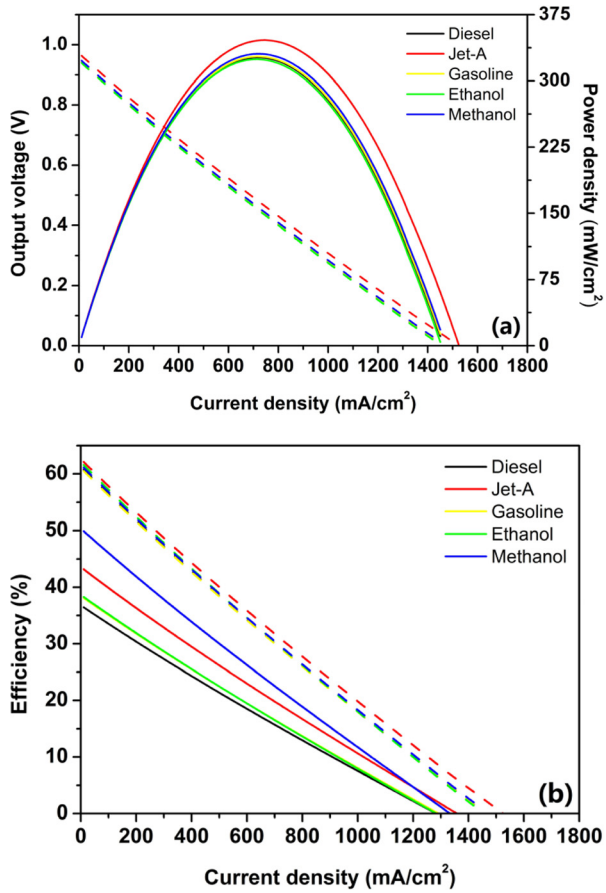

FIG. 8. (a) Calculated SOFC's performance and (b) calculated efficiency of SOFC and APU system (solid line: system's net efficiency; dashed line: SOFC's efficiency) for different types of fuels.

without heat loss. Heat consumed in the BoPs is for pre-heating of air, fuel, and water. The energy required to pre-heat air, fuel, and water from room temperature to the preset temperature was calculated according to Eq. (18). The flow rates and pre-heating temperatures of different reactants are listed in Table IV. High temperature off-gas which is a mixture of CO_2, H_2O and unreacted H_2 at about 700 °C was assumed to be cooled down to 400 °C in heat exchangers to release heat. The heat produced from the off-gas is calculated according to Eq. (19). Another heat source is the afterburner, which burns unreacted H_2. 15% of the supplied H_2 was unreacted since the utilization factor of H_2 in the SOFC unit was assumed to be 85%. The heat supplied from the afterburner is calculated based on Eq. (20). Figure 9 shows the comparison of heat consumed and heat produced in the APU system operating on different fuels. It shows the produced heat is always more than the consumed heat; thus, the integrated APU system can be thermally self-sustained in the steady state operation. Pre-heating of water to 175 °C superheated steam needs almost 85% of the consumed heat. In heat production, the heat produced from the afterburner is about equivalent to the heat produced from the off-gas. The ratio of consumed heat to produced heat is the highest for diesel (80%) and the lowest for methanol (61%)

$$\Delta\dot{E}_{consumed,i} = \dot{n}_i(H_i^{T_{preset}} - H_i^{T_{room}}), \tag{18}$$

$$\Delta\dot{E}_{off-gas} = \dot{n}_{H_2,off-gas}\Delta H_{H_2}\big|_{400^oC}^{700^oC} + \dot{n}_{CO_2,off-gas}\Delta H_{CO_2}\big|_{400^oC}^{700^oC} + \dot{n}_{H_2O,off-gas}\Delta H_{H_2O}\big|_{400^oC}^{700^oC}, \tag{19}$$

$$\Delta\dot{E}_{afterburner} = 15\%\dot{n}_{H_2+CO,reformate}LHV_{H_2}. \tag{20}$$

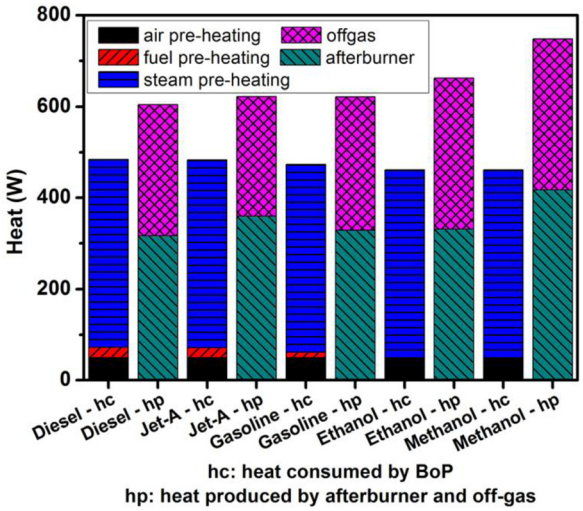

FIG. 9. Heat consumed and heat produced in the APU system operating with different fuels.

IV. CONCLUSIONS

A 1 kW_e integrated APU system consisted of an ATR reformer and a SOFC unit as well as necessary BoP components was analyzed in the present study. Five different types of hydrocarbon fuels, including diesel, Jet-A, gasoline, ethanol, and methanol, were studied as the fuel source for the APU system. The wet reformate compositions produced by reforming of each fuel was experimentally measured. The SOFC's performance was calculated based on a developed and validated model taking into account of concentration polarization, activation polarization, and ohmic loss. It was found that the SOFC's performance and APU system's net efficiency are insensitive to small change of S/C and O_2/C. Channel dimensions have clear influence on the SOFC's performance and the system's net efficiency. In the current density range of 100–400 mA/cm^2, the APU system's net efficiency is about 34%–45%, 30%–40%, 25%–35%, 25%–35%, and 24%–34% for methanol, Jet-A, ethanol, gasoline, and diesel, respectively. Heat produced in the system is always more than heat consumed in the BoP components, so that the system is thermally self-sustainable in the steady state operation.

ACKNOWLEDGMENTS

The support from the startup funding of Harbin Institute of Technology Shenzhen Graduate School (CA45001010) is gratefully acknowledged.

[1]T. S. Lee, J. N. Chung, and Y. C. Chen, Energy Convers. Manage. **52**, 3214 (2011).
[2]M. M. Mench, *Fuel Cell Engines* (John Wiley, New Jersey, 2008).
[3]S. C. Singhal and K. Kendall, *High Temperature Solid Oxide Fuel Cells* (Elsevier Advanced Technology Publishing, Oxford, 2004).
[4]A. Choudhury, H. Chandra, and A. Arora, Renewable Sustainable Energy Rev. **20**, 430 (2013).
[5]X. Xu, P. Li, and Y. Shen, Appl. Energy **108**, 202 (2013).
[6]B. J. Bowers, J. L. Zhao, M. Ruffo, R. Khan, D. Dattatraya, N. Dushman, J. C. Beziat, and F. Boudjemaa, Int. J. Hydrogen Energy **32**, 1437 (2007).
[7]B. Lindström, J. A. J. Karlsson, P. Ekdunge, L. D. Verdier, B. Häggendal, J. Dawody, M. Nilsson, and L. J. Pettersson, Int. J. Hydrogen Energy **34**, 3367 (2009).
[8]S. Ahmed and M. Krumpelt, Int. J. Hydrogen Energy **26**, 291 (2001).
[9]H. Dhingra and B. A. Peppley, J. Power Sources **239**, 527 (2013).
[10]L. Villegas, N. Guilhaume, and C. Mirodatos, Int. J. Hydrogen Energy **39**, 5772 (2014).
[11]S. Yoon, S. Lee, and J. Bae, Int. J. Hydrogen Energy **36**, 10302 (2011).
[12]R. Scenna, T. G. DuBois, and S. Nieh, Fuel **108**, 731 (2013).
[13]X. Xu, S. Zhang, and P. Li, Int. J. Hydrogen Energy **39**, 19593 (2014).
[14]S. R. Yenumala and S. K. Maity, J. Renewable Sustainable Energy **4**, 043120 (2012).
[15]P. Tippawan and A. Arpornwichanop, Bioresource Technol. **157**, 231 (2014).

[16]X. Xu, S. Zhang, X. Wang, and P. Li, Int. J. Hydrogen Energy **40**, 6798 (2015).
[17]N. O. Richards and P. A. Erickson, Int. J. Hydrogen Energy **39**, 18077 (2014).
[18]D. M. Murphy, A. E. Richards, A. Colclasure, W. A. Rosensteel, and N. P. Sullivan, J. Renewable Sustainable Energy **4**, 023106 (2012).
[19]M. Nilsson, Ph.D. thesis, KTH-Royal Institute of Technology, Sweden, 2009.
[20]M. Nilsson, X. Karatzas, B. Lindström, and L. J. Pettersson, Chem. Eng. J. **142**, 309 (2008).
[21]M. Ni, Z. Shao, and K. Y. Chan, Energies **7**, 4381 (2014).
[22]S. M. Hosseini, A. H. Shamekhi, and A. Yazdani, J. Renewable Sustainable Energy **4**, 043107 (2012).
[23]P. Kazempoor, V. Dorer, and F. Ommi, Fuel Cells **10**, 1074 (2010).
[24]W. Doherty, A. Reynolds, and D. Kennedy, Energy **35**, 4545 (2010).
[25]S. H. Chan, K. A. Khor, and Z. T. Xia, J. Power Sources **93**, 130 (2001).
[26]I. Kang, Y. Kang, S. Yoon, G. Bae, and J. Bae, Int. J. Hydrogen Energy **33**, 6298 (2008).
[27]M. Ni, M. K. H. Leung, and D. Y. C. Leung, Energy Convers. Manage. **48**, 1525 (2007).
[28]A. D. Le and B. Zhou, J. Power Sources **182**, 197 (2008).
[29]K. Daneshvar, G. Dotelli, C. Cristiani, R. Pelosato, and M. Santarelli, Fuel Cells **14**, 189 (2014).
[30]H. Liu, P. Li, and K. Wang, Int. J. Hydrogen Energy **38**, 9835 (2013).
[31]P. Li, A. Kotwal, J. L. Sepulveda, R. O. Loutfy, and S. Chang, Int. J. Hydrogen Energy **34**, 6393 (2009).
[32]S. G. Goebel, J. Power Sources **196**, 7550 (2011).
[33]Y. G. Yoon, W. Y. Lee, G. G. Park, T. H. Yang, and C. S. Kim, Electrochim. Acta **50**, 709 (2004).
[34]M. Li, J. D. Powers, and J. Brouwer, J. Fuel Cell Sci. Technol. **7**, 041017-1 (2010).
[35]T. Tanim, D. J. Bayless, and J. P. Trembly, J. Power Sources **245**, 986 (2014).
[36]Y. Lin, R. Ran, Y. Zheng, Z. Shao, W. Jin, N. Xu, and J. Ahn, J. Power Sources **180**, 15 (2008).
[37]S. S. Hsieh and K. M. Chu, J. Power Sources **173**, 222 (2007).